Nanostructures and Photoluminescence Properties of Gd_2O_3:Eu Red-Phosphor Prepared *via* Hydrothermal Route

Kyung-Hee Lee, Yun-Jeong Bae, and Song-Ho Byeon*

College of Environment and Applied Chemistry, Institute of Natural Sciences, Kyung Hee University, Gyeonggi 446-701, Korea
**E-mail: shbyun@khu.ac.kr*
Received August 11, 2008

Various nanostructures (nanorods, nanowires, nanotubes, nanospheres) of $Gd_{0.96}Eu_{0.04}(OH)_3$ have been prepared by hydrothermal reactions at different pHs and temperatures. The aspect ratios of one-dimensional nanostructures are strongly dependent on the solution pH. Subsequent dehydrations of these hydroxides at higher than 500 °C lead to the formation of Gd_2O_3:Eu phosphors with different nanostructures. Interestingly, the shapes of nanorod and nanowire obtained under hydrothermal pressures are retained after the structural transformation from hexagonal $Gd(OH)_3$:Eu to cubic Gd_2O_3:Eu at high temperatures. Gd_2O_3:Eu nanowires can grow up to 20-30 nm in diameter and several tens of micrometers in length. In contrast, the nanotube structure of $Gd(OH)_3$:Eu is collapsed to produce the spherical Gd_2O_3:Eu nanoparticles after dehydration process. A significant change of morphology induced by an adjustment of pH of the initial solution for hydrothermal synthesis of $Gd(OH)_3$:Eu strongly affect the photoluminescence efficiency of Gd_2O_3:Eu phosphor. The relative emission intensity of Gd_2O_3:Eu is reduced with increasing the aspect ratio of nanoparticles, the weakest emission being observed with nanowires of the highest aspect ratio.

Key Words : Phosphor, Nanostructure, Hydrothermal reaction, Photoluminescence

Introduction

The nanostructures such as nanospheres, nanorods, nanotubes, and nanowires are of great importance to applications in diverse fields of science and technology; displays, catalysts, biological sensing, and other optoelectronic devices.[1,2] The selective synthesis of such structures can be achieved by a morphology control in the crystallization process including nucleation and growth. In particular, there are considerable interests in the fabrication of low-dimensional shapes because functional nanomaterials with a restricted dimension offer opportunities for investigating the influence of shape and dimensionality on the optical, magnetic, and electronic properties. Various synthetic approaches have now been developed for many important materials and some structurally unprecedented nanocrystals have been discovered in high quality.

Lanthanide hydroxides and oxides have actively been investigated because of their wide range of applications including dielectric materials for multilayered capacitors, luminescent lamps and displays, solid-laser devices, optoelectronic data storages, waveguides, and heterogeneous catalysts.[3,4] Recently, lanthanide-doped oxide nanoparticles are of special interests as potential materials for an important new class of nanophosphors. When applied for a fluorescent labeling, they present several advantages such as sharp emission spectra, long life times, and resistance against photobleaching in comparison with conventional organic fluorophores and quantum dots.[5,6] For instance, Gd_2O_3 nanopaticle is a promising host matrix for multiphoton and up-conversion excitation.[7,8] The gadolinium oxide doped with Eu^{3+} (Gd_2O_3:Eu) exhibits paramagnetic behavior as well as strong UV and cathode-ray excited luminescences, which are useful in biological fluorescent labeling and display applications, respectively.[9-11] In addition, Gd_2O_3:Eu is a very efficient X-ray and thermoluminescent phosphor.[12]

As a strategy to obtain various inorganic materials in the form of isotropic or anisotropic nanostructures, the solvothermal reaction has frequently been adopted due to its simplicity, high efficiency, and low cost. The hydrothermal synthetic routes to the nanostructures of lanthanide hydroxides are well introduced in the literatures.[13-15] Concerning the Eu^{3-} activator doped phosphor, the nanorod shape of $Gd(OH)_3$:Eu prepared by the hydrothermal reaction was retained after the dehydration into Gd_2O_3:Eu and a difference of about 10 nm in the charge-transfer band position was observed between Gd_2O_3:Eu nanorods and microrods despite the same composition.[16] When we applied the similar technique to synthesize $Gd(OH)_3$:Eu as a precursor for Gd_2O_3:Eu nanophosphor in the present work, a strong pH dependence was observed in particle shape. Various preparation methods have been developed to reduce the reaction temperature and achieve a small particle size of high quality Gd_2O_3:Eu phosphors.[17-20] However, the majority of the cases has focused on the size and shape distributions of the spherical or rod-shape particles. In this paper, we describe a selectively controlled low-temperature hydrothermal synthesis of $Gd(OH)_3$:Eu at different pHs and subsequent dehydration into Gd_2O_3:Eu in the form of nanorods with different aspect ratios, nanowires, nanospheres, and nanotubes. The photoluminescence characteristics of corresponding Gd_2O_3:Eu phosphors were also investigated as a function of morphology and heating temperature.

Experimental

Various nanostructures of $Gd(OH)_3$:Eu (the molar ratio of Eu^{3-} = 0.04) were synthesized at different pHs by using the hydrothermal method. In a typical synthesis, 2.51 g (6.9 mmol) of Gd_2O_3 and 0.10 g (0.29 mmol) of Eu_2O_3 were dissolved in 40 mL of 1.5 M HNO_3 solution. After clear solution was formed by uniform stirring, aqueous KOH (2.0 M) solution was added until the pH of solution was adjusted to be in the range of 8-14 for the formation of colloidal hydroxide precipitates. For the hydrothermal growth of $Gd(OH)_3$:Eu particles, the resulting colloidal mixture was put into a Teflon-lined stainless steel autoclave with a capacity of 100 mL at room temperature. The autoclave was then sealed and maintained at 120-180 °C for 12 h. The solution was continuously stirred during the hydrothermal treatment. After the reaction was completed, the solid product $Gd(OH)_3$:Eu was collected by filtration, washed with distilled water, and dried at 40 °C. Subsequent dehydration of $Gd(OH)_3$:Eu by heating at 500 °C for 5 h yielded Gd_2O_3:Eu oxide. To maintain the morphology of $Gd(OH)_3$:Eu, the heating rate was controlled at 3 °C/min. In order to compare the crystallization, morphology change, and luminescence behaviors at different temperatures, the additional heat treatments for all Gd_2O_3:Eu powders were successively carried out at 700 and 800 °C for 5 h.

The powder X-ray diffraction pattern was recorded on a rotating anode installed diffractometer (18 kW). The Cu Kα radiation used was monochromated by a curved-crystal graphite. Field emission scanning electron microscopy (FE-SEM) was carried out with a Hitachi S-4200 electron microscope operating at 30 kV. Specimens for electron microscope were coated with Pt-Rh for 180 s under vacuum. Transmission electron microscopy (TEM) observations were made with a Philips CM200 operating at 200 kV. High-resolution transmission electron microscopy (HRTEM) was carried out with a JEM3011 electron microscope operating at 300 kV. The photoluminescence (PL) intensity of phosphors was measured at room temperature using a Hitachi F-4500 spectrophotometer with a Xenon flash lamp. The sample loaded on a powder holder provided by Hitachi (the powder samples were not densely packed on this holder) was mounted about 45° to the excitation and source for PL measurement. All samples were analyzed with the same weight and the same slit was used to measure the excitation and emission spectra. The emission spectra were recorded using maximum excitation wavelength. The excitation spectra were measured at the emission wavelength of 610 nm with maximum intensity. As a reference for the comparison of relative intensities, the excitation and emission spectra of commercial Y_2O_3:Eu were measured on the same condition.

Results and Discussion

Several shapes of $Gd(OH)_3$:Eu nanoparticles could be synthesized by facile hydrothermal treatments of colloidal $Gd(OH)_3$:Eu. Thus, the shape selective synthesis of $Gd(OH)_3$:Eu from nanorods with considerably different aspect ratios to nanowires, nanospheres, and nanotubes could be successively achieved with increasing the pH of initial solution for hydrothermal reaction from about 8 to 14. Although the precipitates showing a layered-type morphology were also obtained after hydrothermal treatment at pH < 7, such products showed an X-ray powder diffraction (XRD) pattern quite different from that of $Gd(OH)_3$. In general, the concentration, pH, and temperature of solution strongly influence the transport behavior of constituting ions and the growth behavior of particles in solvothermal synthesis. Among those parameters, the adjustment of pH for hydrothermal reactions was found to play a key role in selectively controlling the morphology of $Gd(OH)_3$:Eu nanostructures in our work. In particular, KOH would have influence on the nucleation and anisotropic growth of particles. $Gd(OH)_3$:Eu particles were obtained in the form of nanorods with large diameters (low aspect ratios) at pH = 8-10, nanowires at pH = 10-11, nanorods with small diameters (high aspect ratios) at pH = 11-12, and the mixture of nanosheets, nanotubes, and nanorods at pH > 13. It is also noted that the nanorods and nanowires were prepared with higher aspect ratios and more uniform morphologies at higher temperature but the nanotubes were preferred at lower temperature.

Figure 1 shows typical XRD patterns of the as-synthesized $Gd(OH)_3$:Eu from hydrothermal process at pH ~ 8, ~11, and ~13 and Gd_2O_3:Eu obtained after heat treatment at 500 °C. All the reflections can be indexed to the hexagonal (space group $P6_3/m$) and the cubic (space group $Ia3$) phases for $Gd(OH)_3$:Eu and Gd_2O_3:Eu respectively, which are in good agreement with the structure data in literatures.[21-23] While $Gd(OH)_3$:Eu obtained at pH = 8.1 is well crystallized (Figure 1a), the increase of solution pH to 10.8 and 12.9 results in a poorer crystallinity as evidenced by relatively weak and broad X-ray diffraction intensity patterns (Figures 1b and 1c,

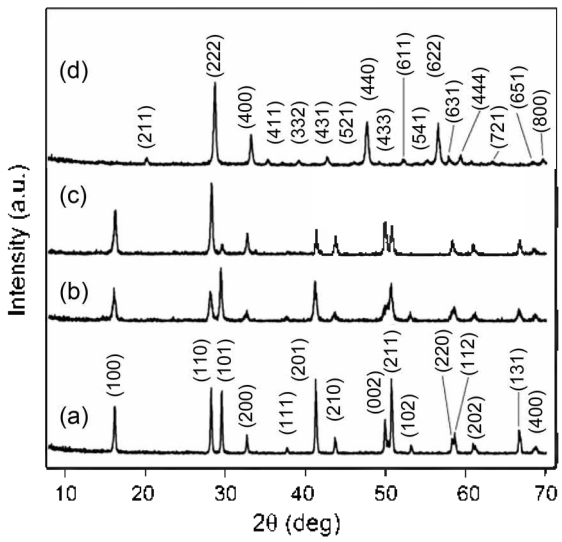

Figure 1. Powder X-ray diffraction patterns of $Gd(OH)_3$:Eu prepared by hydrothermal reaction at 180 °C and pH = (a) 8.1 (nanorods), (b) 12.9 (nanorods), and (c) 10.8 (nanowires) and (d) Gd_2O_3:Eu obtained after dehydration at 500 °C.

respectively). The full-widths at hall-maximum (FWHM) of the (110), (101), (201) reflections of $Gd(OH)_3$:Eu obtained at pH = 8.1 are smaller than one half in comparison with those obtained at pH = 10.8 and 12.9. Furthermore, it is of particular interest that the relative intensities of (110) and (101) diffractions for $Gd(OH)_3$:Eu are significantly different depending on the solution pH for hydrothermal synthesis. The intensity ratios between (110) and (101) reflections of the hydroxides prepared at pH = 8.1 and 12.9 are around 1.0 and 0.5, respectively (Figures 1a and 1b). Similar XRD patterns were observed for $Gd(OH)_3$:Eu oxides which were prepared at different pHs other than 10.8 and the (110)/(101) intensity ratios were typically in the range of 0.5-1.0. These observations are consistent with the previously reported results for $Gd(OH)_3$ without Eu content.[13,14,24] In contrast, such intensity ratio dramatically increased up to ~8 in the XRD pattern of the hydroxide prepared at pH = 10.8 (Figure 1c). This would suggest that the (110) orientation is strongly preferred for $Gd(OH)_3$:Eu prepared at around this pH range. As will be discussed in the next section, $Gd(OH)_3$:Eu particles prepared at pH = 8.1 and 12.9 have a nanorod shape while those prepared at pH = 10.8 show a nanowire shape. Their high resolution transmission electron microscope (HRTEM) images are compared in Figure 2 (The entire images are introduced and discussed in Figures 6 and 8). The fine fringes demonstrate that the as-synthesized $Gd(OH)_3$:Eu nanorods and nanowires are single crystalline. The spacing between fringes along both the rod and wire axes is about 0.32 nm which is close to the interplanar spacing of the (110) plane. This observation, coupled with the exceptionally high (110)/(101) intensity ratio of nanowires, indicates that the growth direction of $Gd(OH)_3$:Eu from nanorods to nanowires is parallel to the (110) planes. $Gd(OH)_3$ nanorods with relatively high aspect ratios have been described as nanowires in the literatures.[13] However, the (110)/(101) intensity ratios in XRD patterns of those hydroxides were in the range of 0.5-1.0, suggesting that they were not essentially nanowires. As far as we know, the XRD pattern of true $Gd(OH)_3$:Eu nanowires, in which the relative intensity of (110) reflection is exceptionally high, would be observed for the first time in the present work.

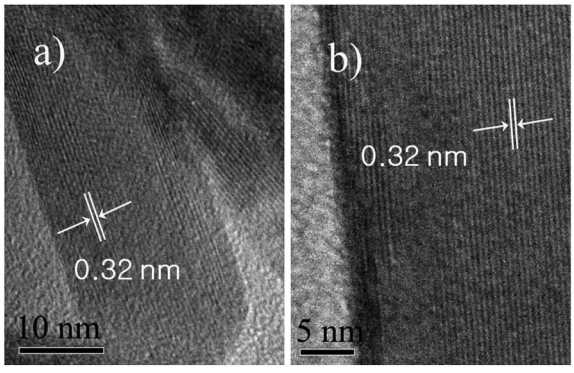

Figure 2. HRTEM photographs of $Gd(OH)_3$:Eu prepared by hydrothermal reaction at 180 °C. pH = (a) 12.9 (nanorods) and (b) 10.8 (nanowires).

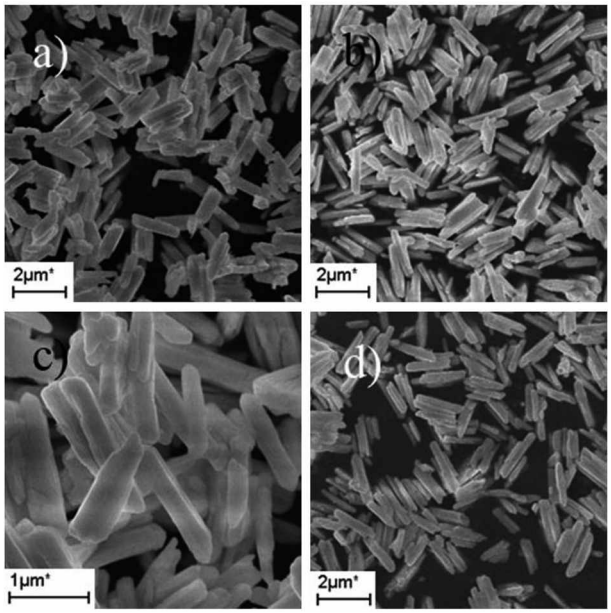

Figure 3. FE-SEM photographs of (a) $Gd(OH)_3$:Eu prepared by hydrothermal reaction at 180 °C, pH = 8.1 and Gd_2O_3:Eu obtained after dehydration at (b and c) 500 °C and (d) 800 °C.

To further understand the influence of pH on the particle shape and size, we have compared the field emission scanning electron microscopy (FE-SEM) and transmission electron microscopy (TEM) images of the as-synthesized $Gd(OH)_3$:Eu and the dehydrated Gd_2O_3:Eu as a function of pH of the initial solution for hydrothermal synthesis.

pH ~ 8: Figure 3 shows FE-SEM images of $Gd(OH)_3$:Eu synthesized by hydrothermal reaction at pH = 8.1 and Gd_2O_3:Eu obtained by subsequent heat treatment at 500 and 800 °C. It can be seen in Figure 3a that the as-synthesized $Gd(OH)_3$:Eu are composed of highly uniform nanorods. The aspect ratio of nanorods is tunable by controlling the experimental conditions of pH, temperature, and concentration (see the next sections). After dehydrating this hydroxide to Gd_2O_3:Eu at high temperatures up to 800 °C, the nanorod shape is completely retained as shown in Figures 3b and 3d. Their average diameter and length from Figure 3c with higher magnification are around 200 nm and 1-1.5 μm, respectively.

pH ~ 9: Figure 4a shows the morphology image of $Gd(OH)_3$:Eu synthesized at pH = 9.0. It is found that this powder also consists of uniform rod-like particles. Compared with those obtained at pH = 8.1, the diameter of as-synthesized $Gd(OH)_3$:Eu nanorods is smaller but the length of nanorods is longer when they were prepared at pH = 9.0. As shown in Figures 4b and 4d, the nanorod structure is not collapsed in Gd_2O_3:Eu oxide obtained after thermal dehydration of the hydroxide at 500 and 800 °C. Their average diameter and length from Figure 4c with higher magnification are around 150 nm and 1.5-2 μm, respectively.

pH ~ 10: During hydrothermal synthesis, we observed that the higher the pH of starting solution is, the smaller diameter of $Gd(OH)_3$:Eu nanorods is induced. In contrast,

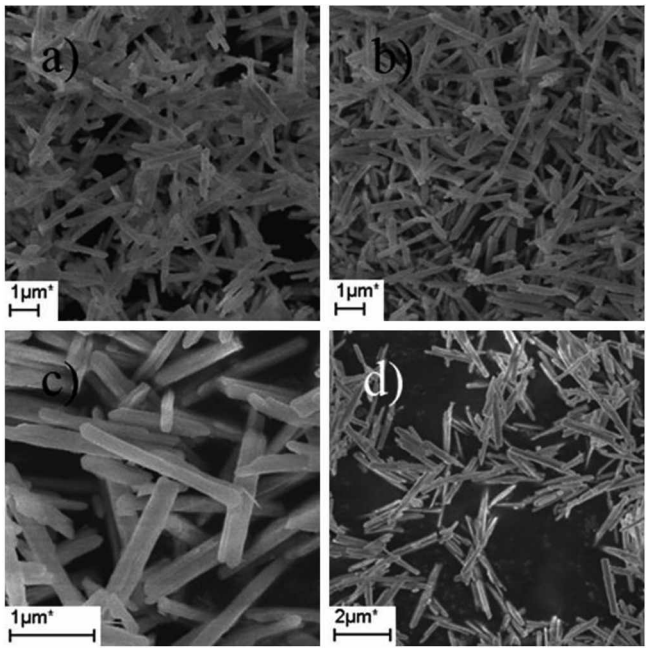

Figure 4. FE-SEM photographs of (a) $Gd(OH)_3$:Eu prepared by hydrothermal reaction at 180 °C, pH = 9.0 and Gd_2O_3:Eu obtained after dehydration at (b and c) 500 °C and (d) 800 °C.

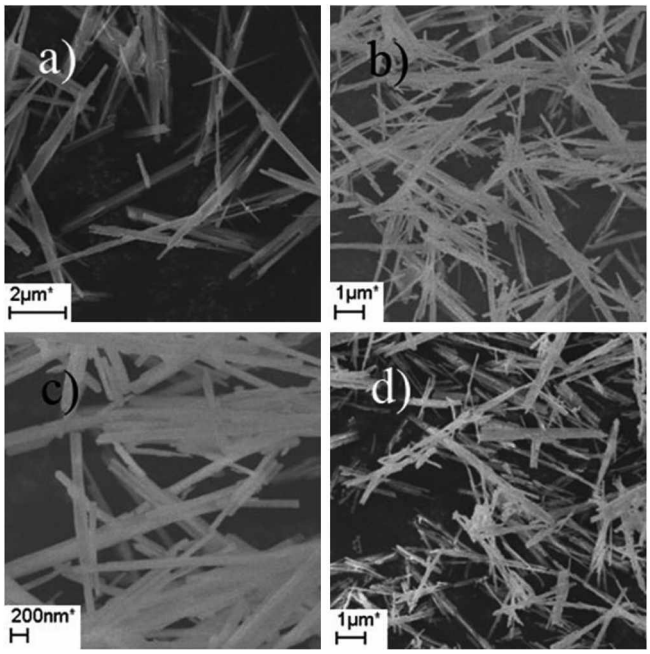

Figure 5. FE-SEM photographs of (a) $Gd(OH)_3$:Eu prepared by hydrothermal reaction at 180 °C, pH = 10.1 and Gd_2O_3:Eu obtained after dehydration at (b and c) 500 °C and (d) 800 °C.

the average length of the nanorods was increased so that the aspect ratio of $Gd(OH)_3$:Eu nanorods becomes higher with the increase of solution pH at the same concentration and reaction temperature. Figure 5 shows typical images of the as-synthesized $Gd(OH)_3$:Eu at pH = 10.1 and its dehydrated oxide Gd_2O_3:Eu. Both compounds exhibit the nanorod structures with average diameter of about 100 nm and length of 3-4 μm.

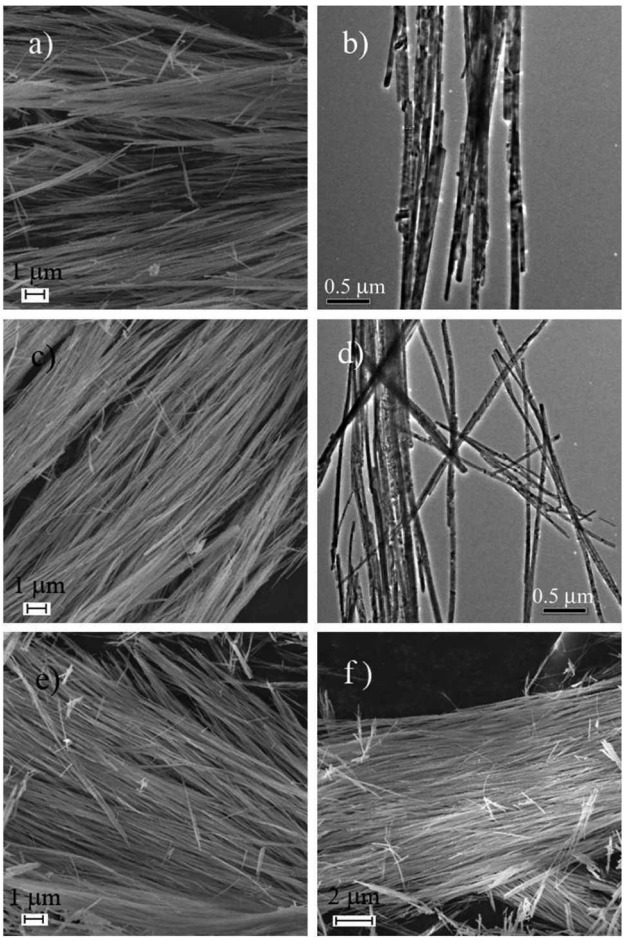

Figure 6. FE-SEM and TEM photographs of (a and b) $Gd(OH)_3$:Eu prepared by hydrothermal reaction at 180 °C, pH = 10.8 and Gd_2O_3:Eu obtained after dehydration at (c and d) 500 °C, (e) 700 °C, and (f) 800 °C.

pH ~ 11: The maximal aspect ratios of $Gd(OH)_3$:Eu and Gd_2O_3:Eu particles were achieved in this pH range. The typical FE-SEM and TEM images of $Gd(OH)_3$:Eu synthesized at pH = 10.8 by hydrothermal method are shown in Figures 6a and 6b, respectively. It is evident from Figure 6a that the as-synthesized $Gd(OH)_3$:Eu is entirely composed of uniform nanowires. Highly anisotropic growth to more uniform nanowires could be achieved by maintaining a higher concentration of the precursors, typically by increasing the amounts of Gd_2O_3 and Eu_2O_3 dissolved the initial HNO_3 solution for hydrothermal synthesis. The temperature was another factor affecting the growth of $Gd(OH)_3$:Eu nanowires. Thus, no nanowires were induced below 120 °C and the nanorods with high aspect ratio were obtained at 120-160 °C. The growth of nanowires of several micrometers in length could be achieved by raising the reaction temperature above 160 °C under auto pressure in the autoclave. Figure 6b with higher magnification suggests that the diameters of nanowires are in the range of 20-30 nm and the lengths can be up to several tens of micrometers. Single crystalline nanowires of hydroxides and oxides have been extensively studied.[25-27] Their formations are related to the fact that the growth rate along one crystallographic direction is signifi-

cantly faster than along the other directions. As observed in XRD pattern (Figure 1c) and HRTEM image (Figure 2b), $Gd(OH)_3$ nanowires are single-crystalline and the growth direction of wire axis is along the (110) plane of the hexagonal unit cell.

By employing a hydrothermal route, uniform single-crystalline $KNbO_3$ nanowires have been obtained.[28] A polymer-assisted hydrothermal synthesis of single crystalline tetragonal perovskite PZT nanowires has also been carried out.[29] However, a direct hydrothermal synthesis of Gd_2O_3:Eu oxide nanowires was unsuccessful in the present work because of high stability of the hydroxide form at high pH conditions. Instead, Gd_2O_3:Eu nanowires could be obtained *via* dehydration of hydrothermally synthesized hydroxide form. In Figures 6c and 6d, we showed the FE-SEM and TEM images of Gd_2O_3:Eu nanowires converted by thermal treatment of $Gd(OH)_3$:Eu nanowires at 500 °C. It is interesting that the nanowire shape of the hexagonal hydroxide is retained after the structural transformation into the cubic oxide. The nanowire morphology of Gd_2O_3:Eu is maintained even after heat treatment up to 700 and 800 °C as shown in Figures 6e and 6f, respectively.

pH ~ 12: Further addition of KOH solution to adjust the pH to higher than 11 significantly reduced the aspect ratio of $Gd(OH)_3$:Eu particles to produce essentially nanorods. The XRD pattern of this hydroxide was quite similar to Figure 1b, the (110)/(101) intensity ratio being close to 0.7. It was suggested that the high OH^- ion concentration is preferable for the high aspect ratio but greatly reduce the ionic motion for the one-dimensional growth.[13] This would imply that an optimal pH condition is required for the growth of true nanowires with high aspect ratio. Figure 7a shows a FE-SEM image of the as-synthesized $Gd(OH)_3$:Eu powder by hydrothermal reaction at pH = 12.1. Although the particle shapes are uniform and wire-like, the aspect ratio is significantly decreased in comparison with that of true nanowires (Figure 6) prepared at pH = 10.8. The morphology images of Gd_2O_3:Eu obtained by dehydrating this hydroxide also exhibit the nanorod shapes (Figure 7b and 7d), indicating the maintenance of morphology after thermal treatment at high temperatures. The diameter and length of rigid nanorods from Figure 7c are in the range of 20-30 nm and 2-3 μm, respectively.

pH ~ 13: Compared with those prepared at lower pH ranges, the morphology of $Gd(OH)_3$:Eu obtained from hydrothermal reaction at pH ~ 13 strongly depends on the reaction temperature; the formation of nanowires is not induced but instead both nanorod and nanotube structures are in competition in this pH range. The formation of nanorods with low aspect ratio are preferred at higher than 160 °C while the nanotubes are mainly obtained at lower than 140 °C. When the hydrothermal reaction is carried out with the initial solution of pH = 12.9, the $Gd(OH)_3$:Eu crystallites synthesized at 180 °C display the uniform morphology of nanorods with

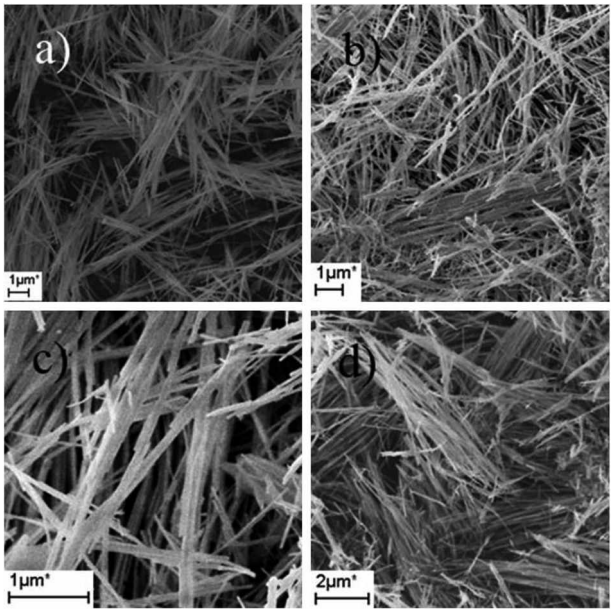

Figure 7. FE-SEM photographs of (a) $Gd(OH)_3$:Eu prepared by hydrothermal reaction at 180 °C, pH = 12.1 and Gd_2O_3:Eu obtained after dehydration at (b and c) 500 °C and (d) 800 °C.

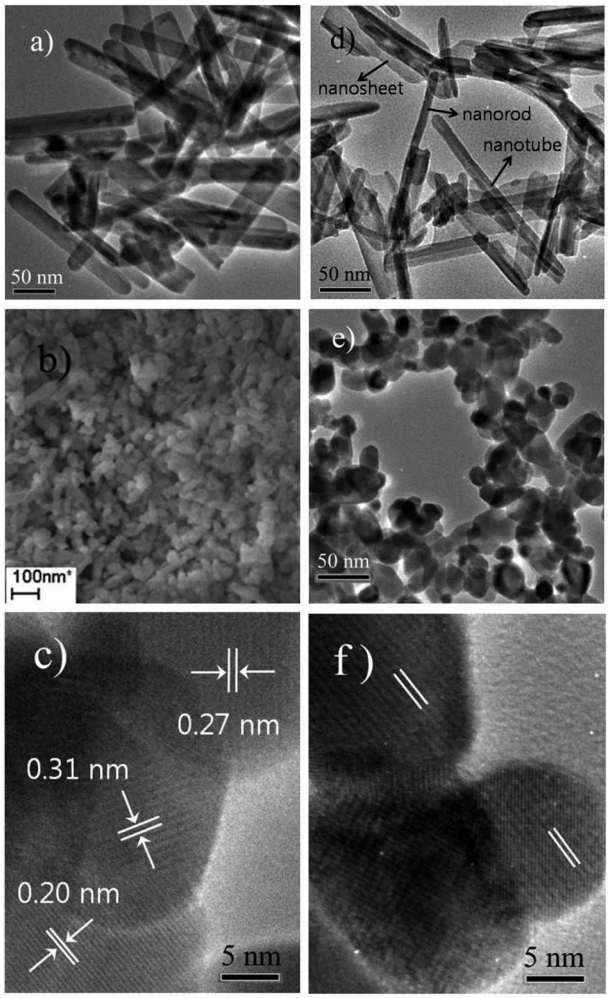

Figure 8. FE-SEM and TEM photographs of (a) $Gd(OH)_3$:Eu prepared by hydrothermal reaction at 180 °C, pH = 12.9 and (b and c) Gd_2O_3:Eu obtained after dehydration at 500 °C. TEM photographs of (d) $Gd(OH)_3$:Eu prepared at 120 °C, pH = 12.9 and (e and f) Gd_2O_3:Eu obtained after dehydration at 500 °C.

20-30 nm in diameter and 200-300 nm in length (Figure 8a). On the other hand, the mixture of nanorods, nanotubes, and nanosheets is produced when $Gd(OH)_3$:Eu is synthesized at 120 °C. Figure 8d shows that the nanotubes have outer diameters less than 30 nm and lengths of 150-200 nm. The nanorods have the aspect ratio smaller than that prepared 180 °C. Considering that the nanosheets are also observed, the formation of sheet-structure is likely followed by the formation of nanotubes at a lower temperature, which in turn grows to more stable nanorods at a higher temperature. The optimal condition to synthesize uniform nanotubes of $Gd(OH)_3$:Eu is strongly dependent on the concentration of KOH and temperature.

In contrast to the observations in other nanorods prepared at lower pHs, the morphology of $Gd(OH)_3$:Eu nanorods obtained at this pH range was not retained after the thermal transformation into Gd_2O_3:Eu. Figures 8b and 8c are the FE-SEM and TEM images of Gd_2O_3:Eu obtained from heat treatment of $Gd(OH)_3$:Eu nanorods at 500 °C. They are all quasi-spherical nanoparticles with size of 30-60 nm. The observed fine fringes are associated with the regular crystalline lattice. The spacings between fringes, 0.32, 0.27, and 0.20 nm are close to the interplanar spacing of the (220), (400), and (440) plane of cubic cell, respectively. The origin of collapse of this nanorod shape is not straightforward. If we consider that the nanosheet, nanorod, and nanotube morphologies are in competition for $Gd(OH)_3$:Eu around this pH range, such collapse would be attributed to a metastable nanorod structure.

Many different strategies for the synthesis and characterization of inorganic nanotubes have been reported extensively in the recent literature.[30] In the majority of the cases, the nanotube structures are induced by a rolling of single sheets from the layered lattices. Some oxide nanotubes have been synthesized by employing a hydrothermal technique. For instance, the hydrothermal synthesis of single-crystalline α-Fe_2O_3 nanotubes has been accomplished.[31] When the direct synthesis of oxide nanotubes is difficult, a precursor prepared by hydrothermal reaction can be used under the appropriate conditions. Highly crystalline TiO_2 nanotubes were synthesized by hydrogen peroxide treatment of low crystalline TiO_2 nanotubes prepared by hydrothermal methods.[32] In particular, CeO_2 nanotubes have been prepared by the controlled annealing of the as-synthesized $Ce(OH)_3$ nanotubes from hydrothermal synthesis.[33] A similar behavior was accordingly expected for $Gd(OH)_3$:Eu and we explored a thermal dehydration of $Gd(OH)_3$:Eu nanotubes to Gd_2O_3:Eu nanotubes. Unfortunately, $Gd(OH)_3$:Eu nanotubes were collapsed into spherical nanoparticles, no Gd_2O_3:Eu nanotubes being obtained after dehydration at 500 °C. As shown in Figures 8e, relatively regular Gd_2O_3:Eu particles are all quasi-spherical and the average particle size is close to 10-40 nm. Observation of the fine fringes in Figure 8f supports a formation of regular crystalline lattice. The nanotubes of cubic Gd_2O_3:Eu, which is not a lamella structure, will require numerous defects and twin orientation relationships, which is energetically unfavorable, during rearrangement for the structural transformation. The difference in strain and curvature between the outer and inner surfaces of nanotubes can induce a different contraction tensions around defects and twins. This torsion would consequently lead to a collapse of tube structure with increasing temperature.

pH ~ 14: The hydrothermal reaction at this pH range resulted in $Gd(OH)_3$:Eu nanorods with low aspect ratios. This hydroxide was not well crystallized and the rod shape was not completely retained after thermal dehydration into Gd_2O_3:Eu. Instead, the mixture of nanospheres and nanorods was obtained.

It is generally expected that the highly anisotropic shapes of nanoparticles would collapse when they transform into a different structure of phase by heat treatment.[34] In this respect, it is noted that the nanorods with large diameters and nanowires of $Gd(OH)_3$:Eu are retained after the transformation into Gd_2O_3:Eu structure by heat treatment up to 800 °C. The structural transformation from hexagonal $Gd(OH)_3$:

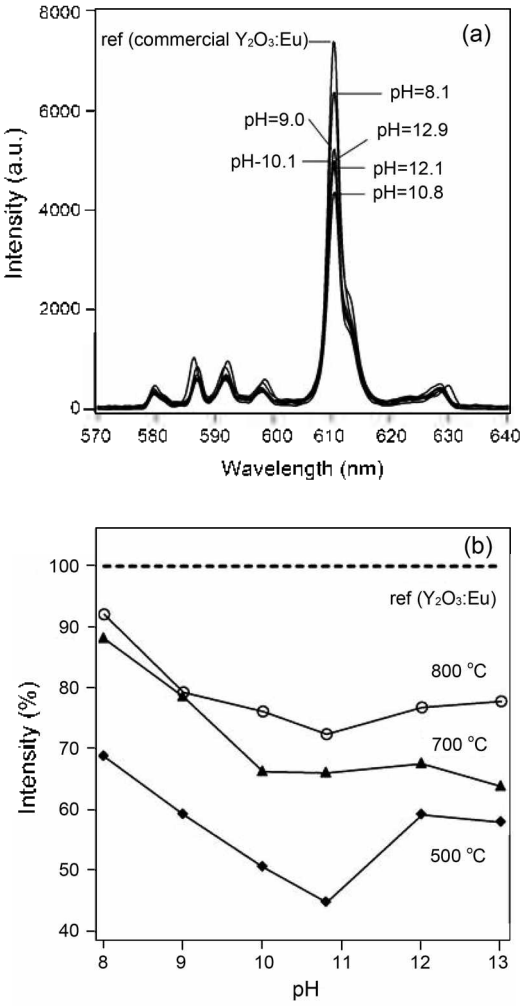

Figure 9. (a) PL emission spectra of Gd_2O_3:Eu obtained after dehydration of $Gd(OH)_3$:Eu at 800 °C. PL emission spectrum of commercial Y_2O_3:Eu is also compared as a reference. (b) Comparison of the relative PL emission intensity of Gd_2O_3:Eu phosphors obtained after heat treatment for 5 h as a function of the solution pH for the hydrothermal synthesis. All intensities were measured as values relative to that of commercial Y_2O_3:Eu.

Eu to cubic Gd_2O_3:Eu proceeds through the formation of intermediate monoclinic GdOOH:Eu. If we consider that the single-crystalline character of $Gd(OH)_3$ nanorods are retained in GdOOH,[35] a sequential transformation from hexagonal to monoclinic and finally to cubic structure, rather than an abrupt transformation, could be responsible for the maintenance of anisotropic rod- and wire-shapes in Gd_2O_3:Eu. The hydrothermal method for the synthesis of $Gd(OH)_3$:Eu consequently provides a selective route to the nanostructures of red-emitting Gd_2O_3:Eu phosphor. In contrast, no shape was retained in the mixture of nanosheets, nanotubes, and nanorods obtained at high pH range but the spherical morphologies were mainly induced after dehydration into Gd_2O_3:Eu. A competition of three morphologies would lead to an unstable nanostructure which is easily collapsed during conversion from $Gd(OH)_3$:Eu to Gd_2O_3:Eu at high temperature.

The optical characteristics and performances of nanometer-sized phosphor materials are generally dependent on their size and morphologies. Therefore, the effect of morphology on the photoluminescence (PL) intensity of Gd_2O_3:Eu phosphor was examined in an attempt to provide an insight for a particle shape of the oxide nanophosphor with high PL efficiency. Indeed, several repeated measurements of the photoemission spectra of Gd_2O_3:Eu with different aspect ratios supported that a systematic difference in PL intensity is induced as a function of the morphology of Gd_2O_3:Eu particles. Figure 9a compares the PL emission spectra of Gd_2O_3:Eu phosphors as a function of the pH value at which corresponding hydroxide precursors were synthesized by hydrothermal reaction. For comparison, the emission intensity measured from a commercial Y_2O_3:Eu is also plotted as a reference in the figure. The intense emission at 610 nm is associated with the $^5D_0$-$^7F_2$ transition of the Eu^{3+} ion.[36] As shown in this figure, Gd_2O_3:Eu oxide from the hydroxide prepared at pH = 8.1 exhibits strong emission whose intensity is close to 90% in comparison with that of commercially available Y_2O_3:Eu. It is noted that the commercial Y_2O_3: Eu phosphor is generally sintered at temperature above 1300 °C. An adoption of hydrolysis technique using urea for the synthesis of Y_2O_3: Eu also requires the firing temperature of 1150-1400 °C to achieve an optimum luminescent property.[37-39] It is accordingly notable that the emission intensity of Gd_2O_3:Eu nanorods obtained at 800 °C is comparable with that of commercial Y_2O_3: Eu. In Figure 9b, the pH dependent PL intensities of Gd_2O_3:Eu phosphors, which were obtained from several repeated measurements, are summarized as a function of the dehydration temperature of corresponding hydroxide precursors. The emission intensity of Gd_2O_3:Eu exhibits a minimum value when the pH for hydrothermal synthesis of the hydroxide increases. The aspect ratio of $Gd(OH)_3$:Eu (or Gd_2O_3:Eu) is enhanced with increasing the solution pH from ~8 to ~11 that is the optimal for the formation of nanowires. In contrast, the PL emission intensity of Gd_2O_3:Eu is monotonically reduced with increase of the aspect ratio in this pH range. The lowest emission is observed with the nanowires (pH ~ 11) of the highest aspect ratio. The intensity of Gd_2O_3:Eu nanowires obtained after dehydration at 800 °C is close to 70% in comparison with that of commercial Y_2O_3:Eu. When pH > 11, the aspect ratio of Gd_2O_3:Eu nanorods is decreased again and then the PL emission intensity is enhanced.

Correlating the particle morphology to PL behavior, the emission intensity of Gd_2O_3:Eu decreases when the aspect ratio becomes larger. One of the origins for such a correlation could be a difference in the surface area of particles. The surface defects would be expected to increase as a consequence of higher aspect ratios, giving rise to larger surface area of crystallites. Some of these defects may act as nonradiative recombination centers and therefore, can be a reason for a decrease of the emission intensity observed in higher aspect-ratio-particles. However, the observation that the emission intensity of nanowires is lower than that of spherical nanoparticles with larger surface area is not in agreement with this behavior. Compared with well crystallized nanospheres (Figures 8c and 8f), the high concentration of stacking faults and twins in the surface of nanowires could results in the lower PL intensity. Furthermore, the optimum Eu activator concentration could be dependent on the particle shape with nanometer size. The determination of concentration quenching range and the surface modifications are in progress for Gd_2O_3:Eu nanowires.

Conclusion

Variable-aspect-ratio, single-crystalline, and one-dimensional nanostructures (nanorods and nanowires) of red-emitting Gd_2O_3:Eu phosphor were prepared by selective hydrothermal synthesis of $Gd(OH)_3$:Eu at different pHs and subsequent dehydration at high temperatures. In particular, this method for the synthesis of Gd_2O_3:Eu nanowires is quite simple and facile. No catalyst is required to serve as the energetically favorable site for the absorption of reactants. No template is added to direct the growth of nanowires. The aspect ratios of phosphor particles are tunable by simply adjusting the pH of the initial solution for hydrothermal synthesis of $Gd(OH)_3$:Eu. A significant change of the aspect ratio strongly affects the photoluminescence efficiency of Gd_2O_3:Eu phosphor. Thus, the selective control of $Gd(OH)_3$: Eu morphology provides a strategy for the selective control of one-dimensional oxide nano-phosphor Gd_2O_3:Eu.

Acknowledgments. This research was supported by the Kyung Hee University Research Fund in 2008.

References

1. Hu, J.; Odom, T. W.; Lieber, C. M. *Acc. Chem. Res.* **1999**, *32*, 435.
2. Kazes, M.; Lewis, D. Y.; Ebenstein, Y.; Mokari, T.; Banin, U. *Adv. Mater.* **2002**, *14*, 317.
3. Guangian, X.; Jimei, X. *New Frontiers Rare Earth Science and Application*; Academic Press: New York, 1985.
4. Cuif, J. P.; Rohart, E.; Macaudiere, P.; Bauregard, C.; Suda, E.; Pacaud, B.; Imanaka, N.; Masui, T.; Tamura, S. *Binary Rare Earth Oxides*; Kluwer Academic Publishers: Dordrecht, 2004.
5. Beaurepaire, E.; Buissette, V.; Sauviat, M.-P.; Mercuri, A.; Martin,

J.-L.; Lahlil, K.; Giaume, D.; Huignard, A.; Gacoin, T.; Boilot, J.-P.; Alexandrou, A. *Nano Lett.* **2004**, *4*, 2079.
6. Louis, C.; Bazzi, R.; Marquette, C. A.; Bridot, J. L.; Roux, S.; Ledoux, G.; Mercier, B.; Blum, L.; Perriat, P.; Tillement, O. *Chem. Mater.* **2005**, *17*, 1673.
7. Hirai, T.; Orikoshi, T. *J. Colloid Interface Sci.* **2004**, *269*, 103.
8. Guo, H.; Dong, N.; Yin, M.; Zhang, W.; Lou, L.; Xia, S. *J. Phys. Chem. B* **2004**, *108*, 19205.
9. Blasse, G.; Grabmaier, B. C. *Luminescent Materials*; Springer: Berlin, 1994.
10. Nichkova, M.; Dosev, D.; Gee, S. J.; Hammock, B. D.; Kennedy, I. M. *Anal. Chem.* **2005**, *77*, 6864.
11. Goldys, E. M.; Krystyna, D.-T.; Jinjun, S.; Dosev, D.; Kennedy, I. M.; Yatsunenko, S.; Godlewski, M. *J. Am. Chem. Soc.* **2006**, *128*, 14498.
12. Rossner, W.; Grabmaier, B. C. *J. Lumin.* **1991**, *48/49*, 29. Rossner, W. *IEEE Trans. Nucl. Sci.* **1993**, *40*, 376.
13. Wang, X.; Li, Y. *Angew. Chem. Int. Ed.* **2002**, *41*, 4790.
14. Wang, X.; Sun, X.; Yu, D.; Zou, B.; Li, Y. *Adv. Mater.* **2003**, *15*, 1442.
15. Wang, X.; Li, Y. *Chem. Eur. J.* **2003**, *9*, 5627.
16. Chang, C.; Kimura, F.; Kimura, T.; Wada, H. *Mater. Lett.* **2005**, *59*, 1037.
17. Yan, M. F.; Huo, T. C. D.; Ling, H. C. *J. Electrochem. Soc.* **1987**, *134*. 493.
18. Shea, L. E.; McKittrick, J.; Lopez, O. A. *J. Am. Ceram. Soc.* **1996**, *79*, 3257.
19. Ravichandran, D.; Roy, R.; White, W. B. *J. Mater. Res.* **1997**, *12*, 819.
20. Erdei, S.; Roy, R.; Harshe, G.; Juwhari, S.; Agrawal, H. D.; Ainger, F. W.; White, W. B. *Mater. Res. Bull.* **1995**, *30*, 745.
21. JCPDS card 83-2037.
22. Buijs, M.; Meyerink, A.; Blasse, G. *J. Lumin.* **1987**, *37*, 9.
23. Kevorkov, A. M.; Karyagin, V. F.; Munchaev, A. I.; Uyukin, E. M.; Bolotina, N. B.; Chernaya, T. S.; Bagdasarov, Kh. S.; Simonov, V. I. *Crystallography Reports* **1995**, *40*, 23.
24. Louis, C.; Bazzi, R.; Flores, M. A.; Zheng, W.; Lebbou, K.; Tillement, O.; Mercier, B.; Dujardin, C.; Perriat, P. *J. Solid State Chem.* **2003**, *173*, 335.
25. Sharma, S.; Sunkara, M. K. *J. Am. Chem. Soc.* **2002**, *124*, 12288.
26. Tang, B.; Zhou, L.; Ge, J.; Niu, J.; Shi, Z. *Inorg. Chem.* **2005**, *44*, 2568.
27. Singh, D. P.; Neti, N. R.; Sinha, A. S. K.; Srivastava, O. N. *J. Phys. Chem. C* **2007**, *111*, 1638.
28. Magrez, A.; Vasco, E.; Seo, J. W.; Dieker, C.; Setter, N.; Forro, L. *J. Phys. Chem. B* **2006**, *110*, 58.
29. Xu, G; Ren, Z.; Du, P.; Weng, W.; Shen, G.; Han, G. *Adv. Mater.* **2005**, *17*, 907.
30. Rao, C. N. R.; Nath, M. *J. Chem. Soc., Dalton Trans.* **2003**, 1.
31. Jia, C.-J.; Sun, L.-D.; Yan, Z.-G.; You, L.-P.; Luo, F.; Han, X.-D.; Pang, Y.-C.; Zhang, Z.; Yan, C. H. *Angew. Chem. Int. Ed.* **2005**, *44*, 4328.
32. Khan, M. A.; Jung, H.-T.; Yang, O.-B. *J. Phys. Chem. B* **2006**, *110*, 626.
33. Tang, C.; Bando, Y.; Liu, B.; Goldberg, D. *Adv. Mater.* **2005**, *17*, 3005.
34. Liang, J. H.; Li, Y. D. *Chem. Lett.* **2003**, *32*, 1126.
35. Chang, C.; Zhang, Q.; Mao, D. *Nanotechnology* **2006**, *17*, 1981.
36. Brecher, C.; Samelson, H.; Lempicki, A.; Riley, R.; Peters, T. *Phys. Rev.* **1967**, *155*, 178.
37. Matijevic, E.; Hsu, W. P. *J. Colloid Interface Sci.* **1987**, *118*, 506.
38. Jiang, Y. D.; Wang, Z. L.; Zhang, F.; Paris, H. G; Summers, C. J. *J. Mater. Res.* **1998**, *13*, 2950.
39. Jing, X.; Ireland, T.; Gibbons, C.; Barber, D. J.; Silver, J.; Vecht, A.; Fern, G.; Trowga, P.; Morton, D. C. *J. Electrochem. Soc.* **1999**, *146*, 4654.